ACS Catalysis

Research Article

pubs.acs.org/acscatalysis

# Charge-Transfer Effects in Ni–Fe and Ni–Fe–Co Mixed-Metal Oxides for the Alkaline Oxygen Evolution Reaction

Michael K. Bates, Qingying Jia, Huong Doan, Wentao Liang, and Sanjeev Mukerjee*

Northeastern University Center for Renewable Energy Technology (NUCRET), Department of Chemistry and Chemical Biology, Northeastern University, 317 Egan Research Center, 360 Huntington Avenue, Boston, Massachusetts 02115, United States

Supporting Information

**ABSTRACT:** Ni–Fe and Ni–Fe–Co mixed-metal oxide (MMO) films were investigated as electrocatalysts for the oxygen evolution reaction (OER) in 0.1 M KOH. In an effort to optimize MMO morphology, aniline was used as a capping agent to produce high-surface-area Ni–Fe–Co films on Raney nickel supports. This catalyst exhibits enhanced mass activity in comparison to the Ni–Fe OER electrocatalysts reported to date. Cyclic voltammetry shows changes in the potential of the $Ni^{2+/3+}$ transitions in Fe- or Co-containing MMO films. In situ X-ray absorption spectroscopy (XAS) analysis confirms that Fe acts to stabilize Ni in the 2+ oxidation state, while Co facilitates oxidation to the 3+ state. The results of this study support the recent claims that Fe (not Ni) is the OER active site. The OER enhancement of the ternary Ni–Fe–Co catalyst results from two effects: (1) the charge-transfer effects of Co result in the formation of the conductive $Ni^{III}OOH$ phase at lower overpotential, thus activating the Fe sites which are otherwise inaccessible to electron transfer in the nonconductive $Ni^{II}(OH)_2$ host lattice, and (2) XAS analysis shows that the presence of Co effectively "shrinks" the Ni and Fe local geometry, likely resulting in an optimized Fe–OH/OOH bond strength. In addition, analysis of heat-treatment effects indicates that calcination at 400 °C improves the OER activity of Ni–Fe–Co but deactivates Ni–Fe. Annealing studies under argon show that MMO surfaces with a hydrated $Ni(OH)_2$ phase and a crystalline NiO phase exhibit nearly identical OER activities. Finally, the morphology of the MMO catalyst film on Raney Ni support provides excellent catalyst dispersion and should result in high active-site utilization for use in technologically relevant gas-diffusion electrodes.

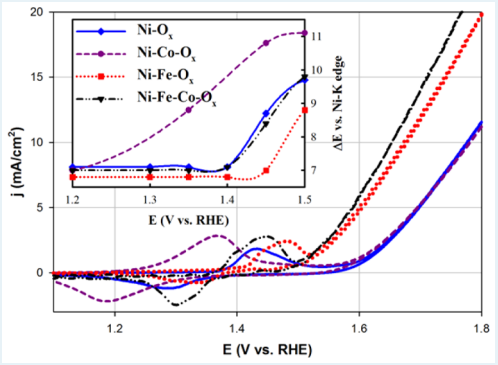


**KEYWORDS:** *electrochemistry, water electrolysis, alkaline oxygen evolution, nickel oxide, X-ray absorption spectroscopy*

## INTRODUCTION

The oxygen evolution reaction (OER) forms a critical corollary to technologically important electrode processes in aqueous and nonaqueous electrolytes. Most important among these is the couple with the hydrogen evolution reaction (HER). In addition, the goal of a reversible oxygen electrode in both aqueous and nonaqueous electrolytes has been the Holy Grail of the electrochemical community, with a direct impact on metal–air batteries. Most of the affordable and sustainable analogues are in the aqueous domain such as the Fe–air system, recognizing that nonaqueous Li–air has one of the highest energy density electrochemical couples. Of the two ends of the pH scale in the aqueous domain, acidic pH as a result of "stability criterion" is restricted to noble metals (especially rare Ir): therefore, the greater focus on alkaline pH.

Recent breakthroughs in alkaline polymer electrolytes (APEs) have sparked increased research into non platinum group metal (non-PGM) electrocatalysts for fuel cells and electrolyzers.[1] Research has identified three main classes of non-PGM electrocatalyst materials for the OER: (a) spinels (with $AB_2O_4$ crystal structure), (b) perovskites (with $ABO_3$ crystal structure), and (c) mixed-metal oxides (typically with $M_xM_{1-x}(OH)_y$ crystal structure). Singh et al.[2] (among many others) have conducted extensive screening of a wide range of spinel OER electrocatalysts with results indicating that catalysts containing both Ni and Fe exhibit the highest OER activity. Perovskites have played a starring role in recent literature because they have shown very promising fundamental properties, such as high "specific activity" (activity normalized to their physical surface area). Unfortunately, the calcination temperatures required for the formation of the perovskite phase (700–1100 °C) also result in significant particle sintering, leading to a physical surface area typically below 1 $m^2/g$, and thus the mass activity (MA) for these samples is lower than the MA reported for mixed-metal oxide (MMO) catalysts.[3] However, Stevenson et al.[4] have recently reported a novel method to produce $La(Ni,Co)O_3$ perovskites with a surface area of ~10 $m^2/g$ which exhibit OER activity rivaling that of PGM catalysts. In contrast to the thermal treatments required to form spinel and perovskite phase catalysts, MMO materials do not require high-temperature heat treatment and can be fabricated by electrochemical deposition or simple hydrothermal methods to produce the transition-metal oxide films.[5]

Received: July 14, 2015
Revised: November 19, 2015
Published: November 20, 2015




DOI: 10.1021/acscatal.5b01481
ACS Catal. 2016, 6, 155–161

Screening of monometallic metal oxide films by Markovic et al.[6] previously indicated that, of the group 3d metals, Ni is the most active for OER. However, Boettcher et al.[7] recently showed that the high apparent activity of "pure Ni oxide" samples in previous reports was due to contamination from trace Fe in the electrolytes. Numerous studies have revealed that Ni−Fe mixed oxides provide a greatly increased OER activity in comparison to pure Ni electrodes—or other binary mixed oxides.[8] Various studies of Ni−Fe systems have shown that catalysts consisting of 60−90 wt % Ni exhibit optimized activity[5a,9] The wide range reported for optimum Ni content is likely due to the range of synthesis methods and heat treatments to which the samples were subjected. In particular, it has been shown that catalysts exhibiting a layered double-hydroxide (LDH) crystal structure are more active than the calcined spinel phase nickel ferrite catalysts. Furthermore, it has been shown that nonconductive FeOOH phases nucleate above a certain Fe content threshold.[9c,10] Until very recently, it was widely assumed that Ni was the OER active site and the role of the Fe in Ni−Fe catalysts was rather ambiguous. The addition of Fe was certainly beneficial in facilitating formation of the LDH phase, thus increasing the effective electrochemical surface area (ECSA). However, recent in situ XAS analysis of Ni−Fe oxides together with DFT calculations by Bell et al.[10a] have indicated that Fe, not Ni, is the OER active site in Ni−Fe catalysts. Furthermore, Boettcher et al.[10b] conducted in situ conductivity testing of $Co_{1-x}Fe_xOOH$ films which indicated that the pure FeOOH films are not conductive until >1.62 V (vs RHE) and, thus, a conductive matrix (of Co or Ni oxide) is required to activate the Fe sites at lower overpotential.

In light of the previous reports mentioned above, this investigation examines in some detail an electrocatalyst comprised of a ternary mixed-metal oxide film of Ni−Fe−Co oxide supported on Raney Ni. This MMO catalyst exhibits the highest OER activity of any electrocatalyst evaluated to date on a mass activity basis. It must be recognized that for any practical OER electrocatalyst its incorporation into a three-dimensional interface provided by gas diffusion media in close concert with ion channels is critical. This is particularly relevant from the perspective of some prior reports where electrodeposited thin films were used.[11]

This report specifically examines the enhanced OER activity of the ternary Ni−Fe−Co MMO over state of the art Ni−Fe LDH materials in the context of aforementioned results of Bell[10a] and Boettcher.[7,10b] In particular the charge-transfer effects of the Co component in the Ni−Fe−Co MMO have been studied in their ability to facilitate oxidation of the insulating $Ni(OH)_2$ to the conductive NiOOH, thus activating the Fe sites in the conductive Ni/Co oxide host at lower overpotential. Furthermore, in situ XAS analysis has been used to reveal that the presence of Co in the MMO film decreases the Ni-centered bond distances. We also show that our XAS results agree with those of Bell et al.;[10a] herein we show that Fe substitutes into the Ni sites, thereby decreasing the average bond distances, presumably resulting in a decrease of the Fe−OH/OOH bond energy and thus leading to optimized adsorbate binding energy. This constitutes a thorough revelation of the likely design elements necessary for enhanced OER electrocatalysis by MMO type materials.

## EXPERIMENTAL SECTION

Raney Ni supported catalysts were synthesized via a modified impregnation method (IM) technique,[12] in the presence of aniline to form a high-surface-area MMO film on the Raney Ni support. To a slurry of Raney Ni (Raney-2800, Sigma-Aldrich) in $H_2O$ (18.2 MΩ Millipore) was added an appropriate amount of metal nitrate salts, or $MoCl_5$ for the Mo/Raney sample (reagent grade, Sigma-Aldrich), to produce a film of 40 wt % MMO on Raney Ni. The high-surface-area MMO film was produced by adding a 10 molar equiv excess (with respect to metal salts) of aniline (Sigma-Aldrich) to the reaction solution and stirring gently for ∼1 h prior to dropwise addition of a 3 molar equiv excess (with respect to metal salts) of sodium borohydride reducing agent (Sigma-Aldrich). The reaction solution was then stirred overnight and subsequently filtered, washed, and dried before heat treatment in a tube furnace. In addition, various carbon-supported binary and ternary Ni alloy electrocatalysts were synthesized by a standard impregnation method (IM) using $NaBH_4$. The carbon support was Vulcan XC-72R (Cabot Corp., Billerica, MA). The support was dispersed in the reaction solution and stirred for at least 1 h, followed by addition of metal nitrate salts and an additional 1 h of stirring. Finally, $NaBH_4$ was added dropwise with vigorous stirring. The solution was stirred for at least 1 h to ensure complete reaction. Both Raney Ni and C supported samples were vacuum-filtered through a Büchner funnel and washed with 500 mL of DI $H_2O$. The Raney Ni supported samples were also washed with 200 mL of acetone to remove any free aniline or aniline oligomers. The solid products were dried in a vacuum oven at 80 °C overnight. Heat-treatment studies were performed in a tube furnace in air for calcination or under argon for annealing.

For electrochemical analysis, inks composed of 3 mL of $H_2O$, 6.95 mL of 2-propanol and 50 μL of 5 wt % ionomer dispersion were mixed with an appropriate amount of catalyst. The ionomer dispersion used was perfluorosulfonic acid−PTFE copolymer (Alfa Aesar, Ward Hill, MA). The inks were sonicated for at least 30 min before a 10 μL aliquot was deposited on the tip of a polished glassy-carbon disk (5.61 mm diameter) to produce a loading of 50 μg of MMO/cm$^2$ for C supported catalysts and 250 μg/cm$^2$ for Raney Ni supported catalysts. MMO samples were compared to an Ir black PGM standard provided by Proton On-Site (Wallingford, CT). The catalyst layers were spin-coated on the RDE tip at 300 rpm using an inverted Pine Instruments rotator to ensure uniform distribution of the catalyst. For examination of the Raney Ni supported catalysts, catalyst layers also contained 50 μg/cm$^2$ Acetylene Black (Chevron) to maximize the dispersion and increase the electronic conductivity. Electrochemical tests were conducted with an Autolab (Ecochemie Inc., Model PGSTAT30) potentiostat/galvanostat. Tests were conducted in a 100 mL three-electrode cell. Alkaline (0.1 M KOH) electrolyte was prepared using potassium hydroxide pellets (semiconductor grade 99.99%, Sigma-Aldrich) and ultrapure $H_2O$ (18.2 MΩ, Millipore). For each test, a freshly made reversible hydrogen electrode (RHE) was used as the reference electrode and a gold flag counter electrode was used to avoid Pt contamination. The glassy-carbon working electrode was rotated using an RDE setup from Pine Instruments. Rotation rates of 2500 rpm were sufficient to remove the $O_2$(g) product from the surface and examine the kinetics well into the OER region. The electrolyte was purged for 30 min with $O_2$(g) prior to testing to mitigate carbonate formation from dissolved $CO_2$ and to simulate the $O_2$-saturated electrolyte of a working electrolysis anode. All reported data were obtained after conditioning electrodes with 20−30 CV scans (100 mV/s from 1 to 1.8 V) or until a stable response was observed. EIS spectra were evaluated at 50 mV intervals from 1.55 to 1.7 V vs RHE (20 kHz to 100 mHz with 10 mV amplitude). The high-frequency resistance was


DOI: 10.1021/acscatal.5b01481
ACS Catal. 2016, 6, 155−161

obtained from EIS data and used to perform *iR* corrections of steady-state OER polarization curves.

XRD characterization was conducted using a Rigaku Ultima IV XRD instrument with a Cu K$\alpha$ source ($\lambda$ = 1.541 Å) operated at 40 kV and 44 mA. $2\theta/\theta$ scans were conducted using a 0.05° step size and 5 s hold per step. XRD analysis was conducted using Rigaku's PDXL software. SEM characterization was conducted using a Hitachi S-4800 FE-SEM instrument. EDS data was collected using EDAX Genesis on the SEM to validate sample elemental composition. XAS measurements were conducted at the X3B beamline of Brookhaven National Laboratories, and analysis was performed using the IFEFFIT suite. Additional details of XAS measurements are provided in the Supporting Information.

## RESULTS AND DISCUSSION

**1. Validation of Metal Trends for OER.** In an effort to validate previous trends of OER activity on transition-metal oxides, we first synthesized monometallic films on the Raney Ni support. Figure 1 shows the results of cyclic voltammetry testing

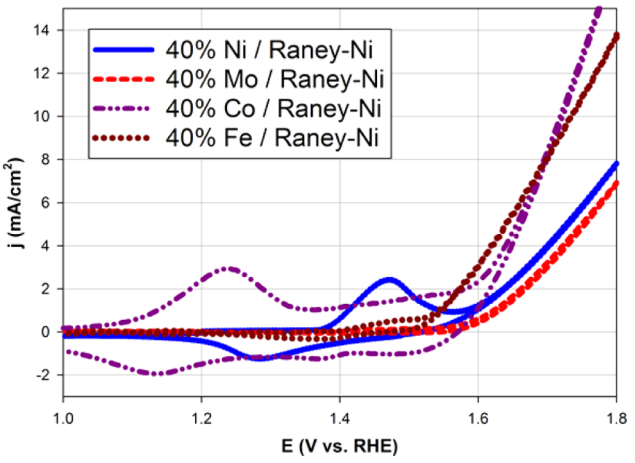


**Figure 1.** CV data (20 mV/s) showing $Ni^{2+/3+}$ redox peaks and OER activity from Raney Ni supported samples. Conditions: 250 $\mu$g/cm$^2$ catalyst loading on GC RDE substrate; tested in $O_2$-purged 0.1 M KOH at room temperature (~23 °C) and 2500 rpm.

on the films of Ni, Mo, Co, and Fe on the Raney Ni support. The results indicate that the Mo surface on Raney Ni did not enhance the OER activity, and the lack of redox peaks on the Mo/Raney sample indicate that the Mo surface may be completely passivating the redox activity of the Raney Ni substrate. Furthermore, the Fe/Raney Ni sample also showed muted $Ni^{2+/3+}$ redox peaks, indicating the presence of an iron-rich surface. It has been previously reported that iron-rich surfaces do not exhibit the OER enhancement typical of mixed Ni−Fe systems.[9c] Finally, it should be noted that the redox peaks observed on the Co/Raney Ni sample occur at a potential much lower than the redox peaks characteristic of the $Ni^{2+/3+}$ transitions. The redox peak potentials observed on the Co/Raney Ni surface are very similar to those reported by Berlinguette et al.[9d] for the $Co^{2+/3+}$ transition. Figure 1 also clearly shows enhancement in OER activity by addition of Fe or Co to the Raney Ni substrate. These results were conducted on unheated samples to avoid the formation of crystalline spinel phase materials.

**2. Comparison of Steady-State OER Activity.** Following identification of the OER enhancement from Fe and Co addition to the Raney Ni support, preliminary MMO composition optimization studies were conducted. Nickel-rich samples with 9:1 Ni:Fe and 8:1:1 Ni:Fe:Co atomic ratios exhibited maximum OER activity. These results support recent literature, which indicates that a Ni-rich composition provides ideal OER activity. Although many recent reports evaluating the fundamental properties of OER catalysts chose to report the MA at overpotentials of 350 or 400 mV (*iR*-comp.), we chose to evaluate OER performance only up to 1.8 V (vs RHE) applied potential, because this translates to full-cell operation below 2 V assuming 100−200 mV cathodic overpotential from the HER catalyst. Figure 2 shows the clear increase in OER activity by

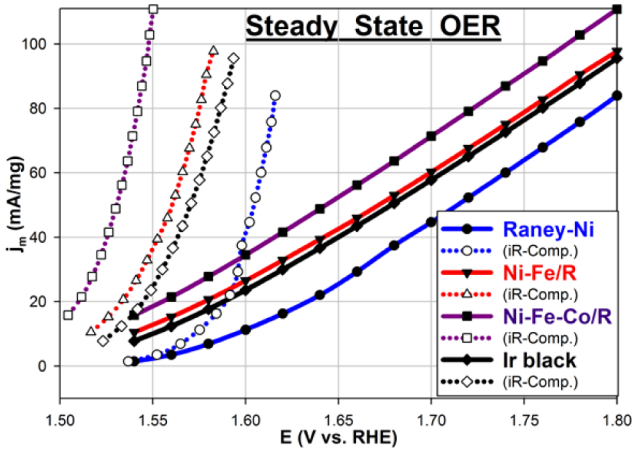


**Figure 2.** Steady-state OER chronoamperometry results. Conditions: 20 mV steps with 1 min hold/step; 0.25 mg/cm$^2$ catalyst loading, tested in $O_2$-purged 0.1 M KOH at room temperature (~23 °C) and 2500 rpm.

adding Ni−Fe and Ni−Fe−Co MMO films to the Raney Ni substrate. This increased activity is evident from both the raw data and *iR*-comp. data. It should be noted that all catalysts reported in Figure 2 exhibited ~36 Ω high-frequency resistance (HFR). The bulk of this resistance can be attributed to the low conductivity (~20 mS/cm)[13] of the 0.1 M KOH electrolyte at ~23 °C. However, calculations[14] based on the geometry of the three-electrode configuration indicate solution resistance on the order of 22 Ω. The EIS results are presented in Figure S1 of the Supporting Information along with a detailed discussion of the analysis and the relative resistivity of the MMO film. However, the nearly identical HFRs of the MMO and Ir black samples suggest that the MMO/Raney Ni catalyst layer exhibits conductivity similar to that of the benchmark Ir black catalyst and thus contributes negligibly to the measured resistance.

In addition to increasing the OER activity beyond that of the Raney Ni substrate, the addition of the MMO films produces catalyst layers which exhibit increased performance in comparison to an Ir black standard provided by Proton On-Site. Furthermore, Figure S2 in the Supporting Information shows the stability of the ternary Ni−Fe−Co/Raney Ni catalyst during 1 h of continuous operation at 1.7 V applied potential (1.54 V *iR*-comp.). During the course of the entire 1 h the average current was 18.2 mA/cm$^2$ with a standard deviation of 0.07 mA/cm$^2$, which translates to an average mass activity of 70 mA/mg over the course of the 1 h test, with a loss of less than 1% after reaching a stable steady state at ~2 min. Although the data are somewhat noisy due to occasional bubble formation on the tip of the working electrode, the durability of this sample is apparent.



DOI: 10.1021/acscatal.5b01481
*ACS Catal.* 2016, 6, 155−161

**Table 1. Comparison of Recently Reported OER Activities under Identical Conditions: 0.1 M KOH @ 25 °C**

| catalyst | size (nm) | mg/cm$^2$ | mA/mg @ 1.55 V *iR*-comp. | ref |
|---|---|---|---|---|
| BSCF perovskites | micrometer | 0.25 | 20 | 3b |
| $LaMO_3$/N-doped-C | 20−50 | 0.05 | 30 | 4 |
| $IrO_2$ nanoparticles | 6 | 0.05 | 40 | 16 |
| Ni−Fe LDH | 20 × 500 plates | 0.07 | 70 | 15 |
| Ni−Fe LDH/CNT | 5 × 50 plates | 0.2 | 80 | 5b |
| Ni−Fe LDH/CQD | 5 × 50 plates | 0.2 | 100 | 5c |
| Ni−Fe−Co/Raney Ni | 2−5 | 0.25 | 110 | this work |

Recently literature has reported Ni−Fe LDH catalysts with extremely high OER MA.[5b,c,15] To our knowledge, the highest MA to date, reported by Song et al.,[15] has resulted from exfoliation of these Ni−Fe LDH materials to form subnanometer films of LDH which were described as 2D networks of $MO_6$ clusters. This exfoliated LDH catalyst material has shown unprecedented MA on the order of 300−400 mA/mg at $\eta$ = 320 mV, although this was in 1 M KOH, as opposed to the 0.1 M KOH standard electrolyte concentration used to more closely simulate the pH ∼13 conditions of commercially available anion-exchange membranes. In addition, these exfoliated LDH nanoflakes were tested at relatively low mass loading (70 $\mu$g/cm$^2$). Under the conditions reported by Song et al.,[13] the utilization of the active sites likely approaches 100%. However, in a real electrode it is very unlikely that the MA of the exfoliated LDH will scale linearly—i.e., active site utilization will be much lower once the catalyst is stacked in a thick film. Thus, although the MA reported by Song et al.[15] acts as an excellent guide to show the inherent OER activity of LDH catalysts, it should be emphasized that optimization of catalyst morphology will be paramount to leverage the high MA of this type of catalyst in technologically relevant gas diffusion electrodes.

The MMO catalyst reported here provides an example of a novel morphology which may allow high active site utilization at higher catalyst loading on a real electrode. As a basis for comparison, Table 1 reports the MA of the leading perovskite, PGM, and MMO catalysts under nearly identical testing conditions. Although Shao-Horn et al.[3b] and Stevenson et al.[4] reported perovskites which exhibited MA approaching that of the Ir PGM standard[16] at high overpotential (350−400 mV), Table 1 emphasizes that the Ni−Fe LDH samples of Song et al.,[15] Gong et al.,[5b] and Kang et al.[5c] exhibit much higher MA at low overpotential. The advantage of the Ni−Fe catalysts results from the very low onset potential for OER on these catalysts. This high OER activity at low overpotential translates into significant energy savings for full-cell water electrolysis using these non-PGM catalysts.

**3. Observations of Charge-Transfer Effects.** Figure 3 shows the $Ni^{2+/3+}$ peaks and OER activity for MMO films on carbon supports. While the C supported samples would not be stable under the high-voltage conditions of an operational OER anode, these samples allow for analysis of the MMO film without contribution from the Raney Ni support. The results indicate that Co facilitates oxidation of $Ni^{2+}$ to $Ni^{3+}$ at lower potentials. In contrast, Fe appears to stabilize the $Ni^{2+}$ oxidation state. It has been noted by Gong et al.[5b] and Bell et al.[9e] that the inclusion of Fe in Ni oxide catalysts appears to create a more disordered local structure, characteristic of the $\alpha$-$Ni(OH)_2$ phase. In addition, Bell et al.[9e] noted that the average oxidation state of Ni in films with Fe was lower than that in pure Ni oxide films—i.e., inclusion of Fe into the Ni oxide film increases the potential at which the $Ni^{2+/3+}$ transition occurs. Furthermore, the effects of Co on the

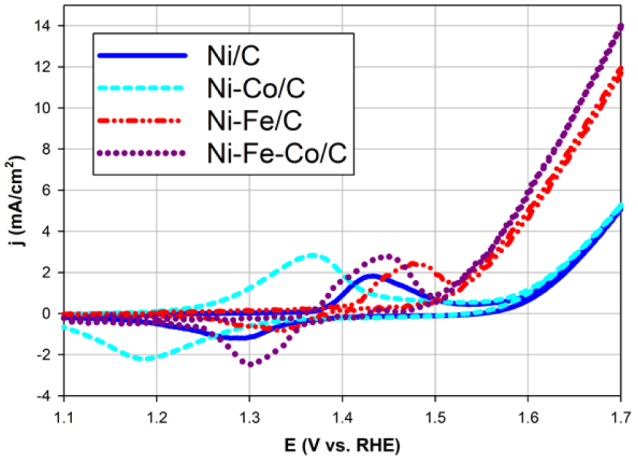


**Figure 3.** CV data (20 mV/s) showing $Ni^{2+/3+}$ redox peaks and OER activity from C-supported samples used for XAS analysis. All samples are 30 wt % MMO/C. Atomic ratios of MMO films are 1:1 Ni:Co, 9:1 Ni:Fe, and 8:1:1 Ni:Fe:Co.

Ni redox peaks in coprecipitated Ni−Co oxide films has been noted by Corrigan et al.[17] In particular, they noted a cathodic shift of the $Ni^{2+/3+}$ redox features in the presence of Co.

It is interesting to note that addition of Co to the Ni oxide film does not appear to enhance the OER activity; however, both samples containing Fe exhibit significantly enhanced OER activity. Boettcher et al.[7] noted that while Fe does increase the conductivity of the Ni oxide film, this effect cannot entirely account for the enhancement of OER activity on Ni−Fe surfaces. Thus, in light of the recent DFT results by Bell et al.[10a] it appears that these data support the assertion that Fe is the active site. While FeOOH alone is not sufficiently conductive to act as a catalyst at low overpotentials, calculations and experiments have shown that Fe sites in a conductive host matrix (Ni or Co oxide) exhibit ideal binding energy with −OH and −OOH intermediates.[10a] Thus, the further OER enhancement of the Ni−Fe−Co catalyst is likely due to activation of the more conductive $Ni^{III}OOH$ phase (in comparison to the non-conductive $Ni^{II}(OH)_2$ phase[7]) at lower overpotential due to charge-transfer effects from the Co component.

**4. Observations of Charge-Transfer Effects from in Situ XAS Analysis.** In an effort to further examine the charge-transfer effects in MMOs, in situ XAS analysis was conducted at Ni, Fe, and Co K-edges on the C supported MMO samples. The XAS data show distinct differences in the potential dependence of the Ni K-edge energy from the various MMO samples. In contrast, upon an increase in the applied potential, no shift in energy is observed at the Fe K-edge (for data collected from 1 to 1.45 V) and the Co K-edge shows only a minor shift in the edge energy (Figures S3 and S4 in the Supporting Information). These results are consistent with previous reports which have also observed


DOI: 10.1021/acscatal.5b01481
*ACS Catal.* 2016, 6, 155−161

that Fe exists in the 3+ oxidation state under OER conditions.[5b,10a] Figure S5 in the Supporting Information shows the Ni K-edge XANES and FT-EXAFS data for all four samples: Ni−($O_x$)/C, Ni−Co−($O_x$)/C, Ni−Fe−($O_x$)/C, and Ni−Fe−Co−($O_x$)/C. However, to focus on the most relevant data, Figure 4a compares the Ni K-edge XANES data from each

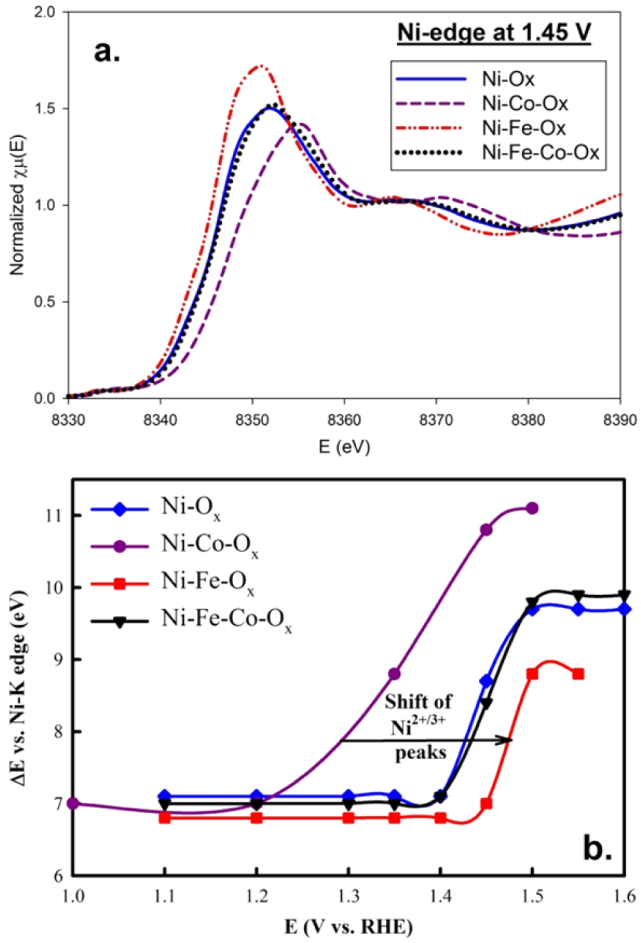


**Figure 4.** Summary of XAS analysis: shifts in Ni K-edge energy due to the presence of Fe and/or Co. (a) Ni K-edge XANES data for various samples at 1.45 V applied potential (potential at which edge-energy shift is most apparent). (b) Graphical representation of shifts in Ni K-edge energy (relative to 8333 eV) for various MMO samples as a function of applied potential. The arrow shows the correlation with the observed shift in $Ni^{2+/3+}$ redox potential.

sample at 1.45 V applied potential, where the difference in oxidation states is most obvious. Figure 4b provides a depiction of the relative shift in the Ni K-edge energy of each sample as a function of applied potential. The results support the CV data shown in Figure 3, which indicate that Fe stabilizes Ni in the 2+ oxidation state, while Co facilitates oxidation to $Ni^{3+}$ at lower applied potential.

Figure 4b shows the shift in Ni K-edge energy relative to the value of 8333 eV for pure Ni foil and emphasizes the charge-transfer effects of Fe and Co in the MMO films. The exact direction of charge transfer (i.e., to/from Ni) is rather ambiguous, due to the structure of these MMO samples. In a typical intermetallic alloy it is presumed that charge donation from the Co to Ni sites would allow oxidation of the Ni sites at lower potential (and vice versa for Ni−Fe charge transfer). However, as these catalysts consist of nonstoichiometric metal oxy hydroxides, they likely interact by indirect charge transfer via the bridging oxygen atoms.

EXAFS fitting of the Ni K-edge data (Table S2 and Figures S6 and S7 in the Supporting Information) shows that (1) for all samples, the Ni K-edge data match very closely the recent results by Bell et al.[10a] indicating that the Ni exists in the γ-NiOOH phase under the high-voltage conditions tested and (2) the insertion of Co leads to contraction of Ni-centered bond distances, including Ni−O and Ni−M (M represents a metal such as Ni, Fe, and/or Co). This effect is caused by the substitution of the $Ni^{2+}$ with $Co^{3+}$ with shorter bond distances due to the higher oxidation state. For a similar crystalline metal oxide, Upton et al.[18] recently reported that strain effects in $NdNiO_3$ facilitate the charge transfer between two elementally different atoms (Ni and Co here) despite the fact that the atoms had been assumed to be isolated from each other (note the long Co−Ni bond distances given by EXAFS (Table S2). Another beneficial role of the strain induced by Co is to increase the electrical conductivity of the MMO. Interestingly, while these changes further increase the OER activity of γ-$Ni_{1-x}Fe_xOOH$, they do not affect the OER activity of γ-NiOOH. This strongly suggests that the Fe is the active site which is responsible for the high OER activities of Ni−Fe and Ni−Fe−Co. Specifically, the shortening of bond distance is expected to result in further OER activity enhancement if Fe is the active site, since Fe is known to overbind OER intermediate adsorbates,[10a] and the strain effects are known to reduce the binding energies between Fe and OER intermediates. On the other hand, it will not increase the OER activity if Ni is the active site, since Ni already binds the OER intermediates too weakly.

**5. Investigations of Heat-Treatment Effects.** Due to the wide range of heat treatments for OER catalysts reported in the literature, additional studies were conducted to evaluate the effects of heat treatment on the Raney Ni and C supported catalyst samples. The OER activity and XRD profiles of the catalyst samples were evaluated to examine the effects of heating the MMO films under argon (annealing) or calcination of the films in an ambient air atmosphere. The results of heat treatment studies on the MMO/Raney Ni samples are presented in Figures S8−S10 and Table S3 in the Supporting Information. For MMO/Raney Ni samples, accurate determination of the local structure of the MMO surface is not possible because XRD results are dominated by diffraction from ordered domains within the Raney Ni substrate. However, electrochemical results from the heat-treatment studies of the Raney Ni supported catalysts provided an interesting qualitative result. Figure 5 shows that the binary Ni−Fe catalyst exhibits enhanced OER activity after annealing in argon but decreased OER activity after calcination in air. In contrast, the ternary Ni−Fe−Co catalyst exhibits increased OER activity after heating to 400 °C under an argon or air atmosphere. While the reason for the increased tolerance to oxidizing heat treatment of the Ni−Fe−Co MMO is not clear, these results suggest a higher stability of the ternary MMO.

In an effort to more clearly identify the phase changes in the active surface, MMO samples on carbon supports were evaluated before and after annealing heat treatment. The calcination heat treatment was not studied for carbon supported MMO catalysts due to the well-known oxidative degradation of carbon at elevated temperatures.

In particular, the investigation of the heated MMO catalyst provides a comparison between the $Ni(OH)_2$ and NiO crystal phases. Numerous recent reports of OER catalysts have


DOI: 10.1021/acscatal.5b01481
ACS Catal. 2016, 6, 155−161

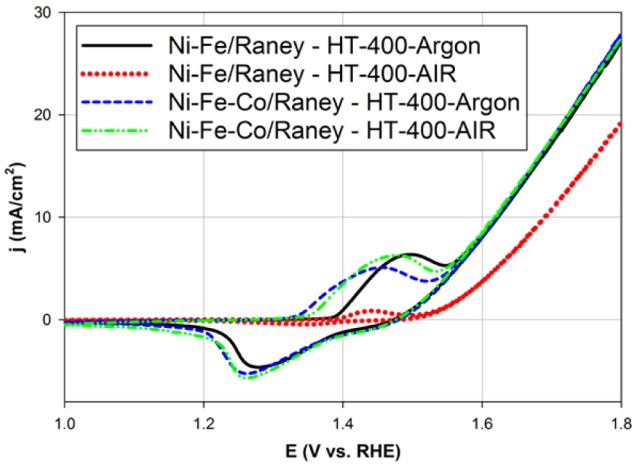


**Figure 5.** CV data (20 mV/s) showing HT effects of Raney Ni supported Ni−Fe and Ni−Fe−Co samples. All samples were heated at 400 °C under argon or air for 30 min.

examined the layered double-hydroxide (LDH) phase.[5b,c,15,19] This LDH structure is essentially a hydrated $\alpha$-$Ni(OH)_2$ crystal structure. The distinction of the LDH phase is that directed anion exchange between the interlayers increases the effective ECSA and facilitates exfoliation of highly active LDH nanoplatelets. Furthermore, until very recently a leading hypothesis for the role of Fe in the enhancement of Ni−Fe OER catalysts was that the $Fe^{3+}$ facilitated the formation of the LDH phase by enhancing anion intercalation in the interlayers to balance the cationic charge of the $[Ni^{2+}_{1-x}Fe^{3+}_{x}(OH)_2]^{x+}$ structure. The results of the heat treatment study indicate that the unheated samples consist primarily of the hydrated $Ni(OH)_2$ phase, while the annealed samples exhibit a more crystalline (i.e., dehydrated) NiO phase. However, the OER activity of both the binary Ni−Fe and ternary Ni−Fe−Co samples does not change significantly with heating. These data show that the OER activity of these MMO catalysts is not dependent on the degree of hydration of the $NiO_x$ phase.

Figure 6a shows that both the binary Ni−Fe and ternary Ni−Fe−Co MMO films exhibited a significant decrease in the redox peak charge upon annealing, indicative of a transition from a hydrated phase to a more crystalline oxide. However, at operating voltages (1.7−1.8 V vs RHE), the OER activity of the annealed samples was very similar to that of the unheated samples. The decreased $Ni^{2+/3+}$ redox charge suggests a decreased ECSA, indicating a phase transition from the hydrated $\alpha$-$Ni(OH)_2$ phase to a dehydrated NiO phase. Figure 6b shows the XRD results for the Ni−Fe sample (XRD results for the Ni−Fe−Co sample can be found in Figure S13 in the Supporting Information). For both the Ni−Fe and Ni−Fe−Co samples, the XRD analysis shows a clear transition from the $Ni(OH)_2$ phase with a crystallite size of 2−3 nm to the NiO phase with a crystallite size of ∼5 nm after annealing in argon. Finally, the inset of Figure 6a examines the $Ni^{2+/3+}$ redox peaks of the heated samples. The inset shows that the redox peak potentials of the Ni−Fe film are observed at potentials higher than those for the ternary Ni−Fe−Co. The increased OER activity of the heated Ni−Fe−Co is apparent in the full-scale plot. This observation is in agreement with the observed shifts in OER activity and $Ni^{2+/3+}$ peak potentials discussed above in reference to Figure 3.

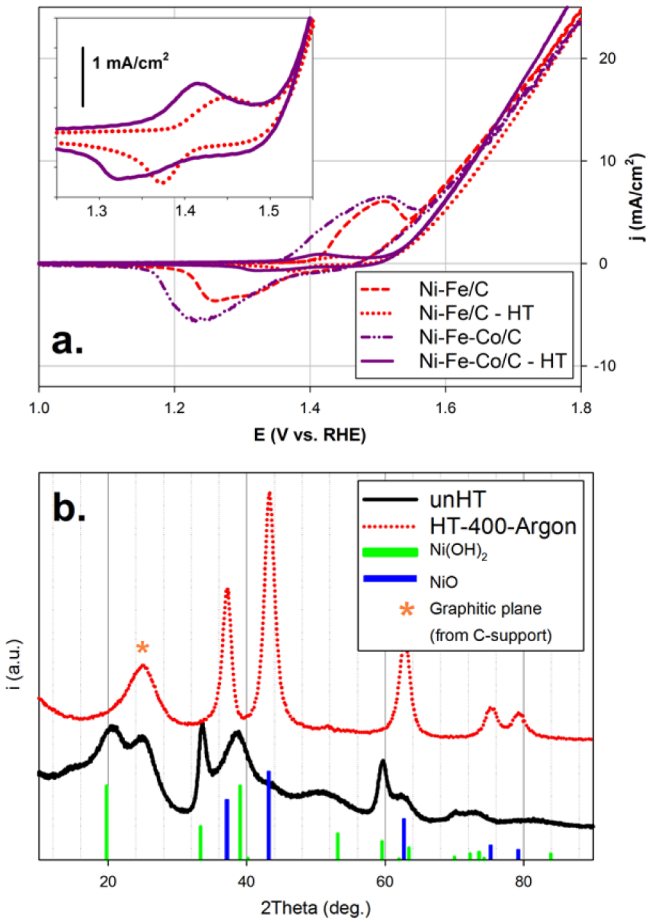


**Figure 6.** (a) CV data (20 mV/s) showing HT effects of C supported Ni−Fe and Ni−Fe−Co samples. Both HT samples were annealed at 400 °C under argon for 30 min. (b) XRD data from Ni−Fe/C sample after annealing heat treatment at 400 °C under argon forming gas. Profile fitting indicates a 2−3 nm crystallite size for the $Ni(OH)_2$ phase in the unheated sample and 5 nm crystallite size for the NiO phase in the heated sample.

## CONCLUSIONS

Binary and ternary mixed-metal oxide (MMO) films on a commercial Raney Ni support were evaluated for alkaline OER activity in 0.1 M KOH at room temperature (∼23 °C). Electrochemical testing in an RDE configuration showed that a ternary Ni−Fe−Co oxide (with 8:1:1 atomic ratio of metals) catalyst exhibited the best OER activity heretofore. The MA was 110 mA/mg at 1.55 V (*i*R-comp.). In addition, the ternary Ni−Fe−Co catalyst showed less than 1% loss of OER activity at 1.7 V applied potential (1.54 V *i*R-comp.) during 1 h of continuous operation. Although a direct comparison is not possible due to the different test conditions, this catalyst is comparable to the best materials presented recently by Jaramillo et al. for alkaline OER.[20] Analysis of the heat treatment conditions reveals that the ternary Ni−Fe−Co sample maintains stable OER activity when heated under inert or oxidizing conditions. In contrast, the binary Ni−Fe catalyst suffered significant deactivation after oxidizing heat treatment. In addition, the high OER activity of the ternary Ni−Fe−Co sample can be rationalized in light of recent in situ XAS and conductivity measurements of Ni−Fe and Co−Fe films.[10a] Recent DFT calculations have proposed that $Fe^{3+}$ sites provide ideal binding energy for the −OH and −OOH OER intermediates, whereas $Ni^{3+}$ sites bind these adsorbates too


DOI: 10.1021/acscatal.5b01481
*ACS Catal.* 2016, 6, 155−161

weakly.[10a] The results of the present study indicate that the most active catalysts are those which contain Fe (Ni−Fe and Ni−Fe−Co). Further enhancement of OER activity from the ternary Ni−Fe−Co sample in comparison to the binary Ni−Fe sample is attributable to conductivity and strain effects. Primarily, the Co component facilitates oxidation of Ni to the more conductive NiOOH phase at lower overpotential, thus effectively activating the Fe sites which are otherwise dormant in the nonconductive $Ni(OH)_2$ phase. In addition, EXAFS fitting of the in situ XAS data shows a decrease in the Ni-centered bond distances in samples containing cobalt. Bell et al.[10a] showed that Fe substitutes into the Ni oxide lattice in $Ni_{1-x}Fe_xOOH$ (for samples with $x < 0.25$). They further indicated that the NiOOH local geometry was not noticeably affected by the replacement of Fe in the Ni sites and that the resulting Fe−metal and Fe−O bond distances were ∼6% smaller than those in a pure FeOOH lattice. Thus, the presence of Co in the MMO films further decreases the Ni(Fe)-centered bond distances and the resulting strain effects are assumed to produce more optimized binding energies between Fe and OER intermediates.

The charge-transfer effects studied in this report present numerous interesting opportunities for tuning the properties of Ni-based catalysts. In particular, Co and Fe doping of NiO semiconducting quantum dots should allow fine tuning of the conduction and valence bands for photoelectrochemical applications. In addition, consideration of these charge-transfer effects may aid the development of higher conductivity Ni−Co supercapacitors or NiMH anodes, or even increased selectivity of Ni-based steam-reforming or hydrogenation catalysts.

## ■ ASSOCIATED CONTENT

### Supporting Information

The Supporting Information is available free of charge on the ACS Publications website at DOI: 10.1021/acscatal.5b01481.

Additional characterization via XRD, SEM, and TEM (PDF)

## ■ AUTHOR INFORMATION


### Corresponding Author

*E-mail for S.M.: s.mukerjee@neu.edu.


### Notes

The authors declare no competing financial interest.

## ■ ACKNOWLEDGMENTS

This work was funded by the Advanced Research Projects Agency-Energy (ARPA-E), U.S. Department of Energy, under Award No. DE-AR0000121, led by Proton OnSite, Wallingford, CT. Use of the National Synchrotron Light Source (beamline X3B), Brookhaven National Laboratory (BNL), was supported by the U.S. Department of Energy, Office of Basic Energy Sciences. This publication was made possible by the Center for Synchrotron Biosciences grant, P30-EB-009998, from the National Institute of Biomedical Imaging and Bioengineering (NBIB). Support from beamline personnel Dr. Erik Farquhar (X3B) is gratefully acknowledged. In addition, technical support provided by Proton OnSite, specifically Drs. Kathy Ayers and Christopher Capuano, are gratefully acknowledged.

## ■ REFERENCES


(1) (a) Merle, G.; Wessling, M.; Nijmeijer, K. *J. Membr. Sci.* **2011**, *377*, 1−35. (b) Varcoe, J. R.; Slade, R. C. *Fuel Cells* **2005**, *5*, 187−200. (c) Varcoe, J. R.; Atanassov, P.; Dekel, D. R.; Herring, A. M.; Hickner, M. A.; Kohl, P. A.; Kucernak, A. R.; Mustain, W. E.; Nijmeijer, K.; Scott, K. *Energy Environ. Sci.* **2014**, *7*, 3135−3191.

(2) (a) Kumar, M.; Awasthi, R.; Sinha, A.; Singh, R. *Int. J. Hydrogen Energy* **2011**, *36*, 8831−8838. (b) Anindita; Singh, A.; Singh, R. *Int. J. Hydrogen Energy* **2010**, *35*, 3243−3248.

(3) (a) Zhu, Y.; Zhou, W.; Chen, Z.-G.; Chen, Y.; Su, C.; Tadé, M. O.; Shao, Z. *Angew. Chem., Int. Ed.* **2015**, *54*, 3897−3901. (b) Grimaud, A.; May, K. J.; Carlton, C. E.; Lee, Y.-L.; Risch, M.; Hong, W. T.; Zhou, J.; Shao-Horn, Y. *Nat. Commun.* 2013, *4*, No.2439;. (c) Risch, M.; Stoerzinger, K. A.; Maruyama, S.; Hong, W. T.; Takeuchi, I.; Shao-Horn, Y. *J. Am. Chem. Soc.* **2014**, *136*, 5229−5232. (d) Suntivich, J.; May, K. J.; Gasteiger, H. A.; Goodenough, J. B.; Shao-Horn, Y. *Science* **2011**, *334*, 1383−1385.

(4) Hardin, W. G.; Mefford, J. T.; Slanac, D. A.; Patel, B. B.; Wang, X.; Dai, S.; Zhao, X.; Ruoff, R. S.; Johnston, K. P.; Stevenson, K. J. *Chem. Mater.* **2014**, *26*, 3368−3376.

(5) (a) Trotochaud, L.; Ranney, J. K.; Williams, K. N.; Boettcher, S. W. *J. Am. Chem. Soc.* **2012**, *134*, 17253−17261. (b) Gong, M.; Li, Y.; Wang, H.; Liang, Y.; Wu, J. Z.; Zhou, J.; Wang, J.; Regier, T.; Wei, F.; Dai, H. *J. Am. Chem. Soc.* **2013**, *135*, 8452−8455. (c) Tang, D.; Liu, J.; Wu, X.; Liu, R.; Han, X.; Han, Y.; Huang, H.; Liu, Y.; Kang, Z. *ACS Appl. Mater. Interfaces* **2014**, *6*, 7918−7925.

(6) Subbaraman, R.; Tripkovic, D.; Chang, K.-C.; Strmcnik, D.; Paulikas, A. P.; Hirunsit, P.; Chan, M.; Greeley, J.; Stamenkovic, V.; Markovic, N. M. *Nat. Mater.* **2012**, *11*, 550−557.

(7) Trotochaud, L.; Young, S. L.; Ranney, J. K.; Boettcher, S. W. *J. Am. Chem. Soc.* **2014**, *136*, 6744−6753.

(8) (a) Li, X.; Walsh, F. C.; Pletcher, D. *Phys. Chem. Chem. Phys.* **2011**, *13*, 1162−1167. (b) McCrory, C. C. L.; Jung, S.; Peters, J. C.; Jaramillo, T. F. *J. Am. Chem. Soc.* **2013**, *135*, 16977−16987.

(9) (a) Chen, J. Y.; Miller, J. T.; Gerken, J. B.; Stahl, S. S. *Energy Environ. Sci.* **2014**, *7*, 1382−1386. (b) Gerken, J. B.; Shaner, S. E.; Massé, R. C.; Porubsky, N. J.; Stahl, S. S. *Energy Environ. Sci.* **2014**, *7*, 2376−2382. (c) Landon, J.; Demeter, E.; İnoğlu, N.; Keturakis, C.; Wachs, I. E.; Vasić, R.; Frenkel, A. I.; Kitchin, J. R. *ACS Catal.* **2012**, *2*, 1793−1801. (d) Smith, R. D.; Prévot, M. S.; Fagan, R. D.; Trudel, S.; Berlinguette, C. P. *J. Am. Chem. Soc.* **2013**, *135*, 11580−11586. (e) Louie, M. W.; Bell, A. T. *J. Am. Chem. Soc.* **2013**, *135*, 12329−12337.

(10) (a) Friebel, D.; Louie, M. W.; Bajdich, M.; Sanwald, K. E.; Cai, Y.; Wise, A. M.; Cheng, M.-J.; Sokaras, D.; Weng, T.-C.; Alonso-Mori, R.; Davis, R. C.; Bargar, J. R.; Nørskov, J. K.; Nilsson, A.; Bell, A. T. *J. Am. Chem. Soc.* **2015**, *137*, 1305−1313. (b) Burke, M. S.; Kast, M. G.; Trotochaud, L.; Smith, A. M.; Boettcher, S. W. *J. Am. Chem. Soc.* **2015**, *137*, 3638−3648.

(11) Lu, X.; Zhao, C. *Nat. Commun.* **2015**, *6*, 6616.

(12) Chan, K.-Y.; Ding, J.; Ren, J.; Cheng, S.; Tsang, K. Y. *J. Mater. Chem.* **2004**, *14*, 505−516.

(13) Gilliam, R. J.; Graydon, J. W.; Kirk, D. W.; Thorpe, S. J. *Int. J. Hydrogen Energy* **2007**, *32*, 359−364.

(14) Newman, J. *J. Electrochem. Soc.* **1966**, *113*, 501−502.

(15) Song, F.; Hu, X. *Nat. Commun.* **2014**, *5*, 4477.

(16) Lee, Y.; Suntivich, J.; May, K. J.; Perry, E. E.; Shao-Horn, Y. *J. Phys. Chem. Lett.* **2012**, *3*, 399−404.

(17) Corrigan, D. A.; Bendert, R. M. *J. Electrochem. Soc.* **1989**, *136*, 723−728.

(18) Upton, M.; Choi, Y.; Liu, J.; Meyers, D.; Middey, S.; Chakhalian, J.; Kim, J.-W.; Ryan, P. J. *arXiv preprint arXiv:1412.0676*, 2014.

(19) Ma, W.; Ma, R.; Wang, C.; Liang, J.; Liu, X.; Zhou, K.; Sasaki, T. *ACS Nano* **2015**, *9*, 1977−1984.

(20) McCrory, C. C. L.; Jung, S.; Ferrer, I. M.; Chatman, S. M.; Peters, J. C.; Jaramillo, T. F. *J. Am. Chem. Soc.* **2015**, *137*, 4347−4357.




DOI: 10.1021/acscatal.5b01481
*ACS Catal.* 2016, 6, 155−161